Proceedings of the ASME 2010 3rd Joint US-European Fluids Engineering Summer Meeting and 8th International Conference on Nanochannels, Microchannels, and Minichannels
FEDSM-ICNMM2010
August 1-5, 2010, Montreal, Canada

FEDSM-ICNMM2010-30729

CONVECTIVE HEAT TRANSFER IN WALL-BOUNDED FLOWS AFFECTED BY SEVERE FLUID PROPERTIES VARIATION: A SECOND-MOMENT CLOSURE STUDY

S. Jakirlić*
Chair of Fluid Mechanics and Aerodynamics[1] and
Center of Smart Interfaces - CSI[2]
Department of Mechanical Engineering
Technische Universität Darmstadt
Petersenstr. 30[1]/32[2], D-64287 Darmstadt, Germany
s.jakirlic@sla.tu-darmstadt.de

R. Jester-Zürker
Voith Hydro Holding GmbH & Co. KG-tts
Alexanderstraße 11, 89522 Heidenheim, Germany
Roland.Jester-Zuerker@voith.com

ABSTRACT

Different flow configurations subjected to increasingly enhanced wall heating were selected to be computationally investigated by means of a differential, near-wall second-moment closure model based on the solution of transport equations for second moments of the fluctuating velocities and temperature, $\widetilde{u_i'' u_j''}$ and $\widetilde{u_i'' \theta}$ respectively. Both Reynolds stress model and heat flux model represent wall-topography free formulations with quadratic pressure-strain term and pressure-temperature-gradient correlation. The transport equations for the turbulent stress tensor and the turbulent heat flux are solved in conjunction with the equation governing a new scale supplying variable, so-called "homogeneous" dissipation rate, Jakirlic and Hanjalic (2002). Such an approach offers a number of important advantages: proper near-wall shape of the dissipation rate profile was obtained without introducing any additional term and the correct asymptotic behaviour of the stress dissipation components by approaching the solid wall is fulfilled automatically without necessity for any wall geometry-related parameter. The configurations considered include fully-developed and developing flows in channel (without and with a sudden expansion) and pipe in conjunction with the scalar transport under conditions of variable fluid properties for which an extensive experimental and numerical (DNS and LES) reference database exists.

INTRODUCTION

The influence of the strong heating of a gas flow (as, e.g., encountered in gas combustors and other high-temperature reactors) is primarily manifested through a severe variations of the fluid properties (density, viscosity) leading consequently to important structural changes. Density reduction and viscosity increase can cause the flow acceleration, which, if sufficiently strong, can suppress turbulence substantially resulting in a laminar flow situation. The most important changes are concentrated in the immediate wall vicinity. The strongest modification of the flow structure occurs in the inner part of the temperature layer.

An increasing number of direct numerical simulations (DNS) and large eddy simulations (LES) provide a detailed database which is indispensable for further development of turbulence models within the RANS (Reynolds-Averaged Navier-Stokes) framework. High resolution of the wall vicinity, being beyond the reach of available measurement techniques, enables detailed insight in the physics of near-wall turbulence, characterized by strong Reynolds-stress and stress-dissipation anisotropy. The deviation from equilibrium conditions in this flow region is further enlarged under conditions of high temperature differences. The main goal of this work is to formulate a near-wall turbulence model based on the solution of the transport equations for unknown second moments of the fluctuating velocity and temperature components (turbulent stresses $\widetilde{u_i'' u_j''}$ and turbu-

*Address all correspondence to this author.

lent heat fluxes $\widetilde{u_i''\theta}$) to be applied to the flows with strong property variations due to intensive heating.

Three flow geometries were presently considered: (1) fully-developed channel flow subjected to a temperature gradient between the upper and lower walls - reference LES was performed by Wang and Pletcher, 1996 (the passive scalar transport configuration - the DNS reference database by Kasagi and Iida, 1999 - served as an introductory case); (2) three backward-facing step flow configurations with increasing heat flux being uniformly supplied through the bottom wall downstream of the step (the reference LES by Avancha and Pletcher, 2002) and (3) a vertical circular tube with air flowing in upward direction (experimentally investigated by Shehata and McEligot, 1998) subjected to three different heating rates - in the third case ($q_w^+ = 0.0045$), for which the DNS database obtained by Satake et al. (2000) and Bae et al. (2006) is also available, laminarization phenomena have been observed.

COMPUTATIONAL MODEL

The continuity, momentum and energy equations governing the steady flow and heat transfer under the variable property conditions read:

$$\frac{\partial(\overline{\rho}\widetilde{U}_i)}{\partial x_i} = 0 \tag{1}$$

$$\frac{\partial\left(\overline{\rho}\widetilde{U}_j\widetilde{U}_i\right)}{\partial x_j} = -\frac{\partial\overline{P}}{\partial x_i} + \frac{\partial}{\partial x_j}\left(\overline{\tau}_{ij}^{\mu} - \overline{\rho}\widetilde{u_i''u_j''}\right) \tag{2}$$

$$\frac{\partial\left(\overline{\rho}C_p\widetilde{U}_j\widetilde{\Theta}\right)}{\partial x_j} = \frac{\partial}{\partial x_j}\left(\overline{\lambda}\frac{\partial\widetilde{\Theta}}{\partial x_j} - \overline{\rho}C_p\widetilde{u_j''\theta}\right) \tag{3}$$

Here $\overline{\tau}_{ij}^{\mu}$ ($= 2\overline{\mu}\widetilde{S}_{ij} - 2\overline{\mu}\widetilde{S}_{kk}\delta_{ij}/3$; $\widetilde{S}_{ij} = 0.5(\partial\widetilde{U}_i/\partial x_j + \partial\widetilde{U}_j/\partial x_i)$) and $\overline{q}_j^{\mu}$ ($= \overline{\lambda}\partial\widetilde{\Theta}/\partial x_j$; with $\overline{\lambda} = C_p\overline{\mu}/Pr$) represent viscous stress tensor and viscous heat flux, whereas turbulent stress tensor $\overline{\tau}_{ij}^{t}$ ($= -\overline{\rho}\widetilde{u_i''u_j''}$) and turbulent heat flux $\overline{q}_j^{t}$ ($= -\overline{\rho}C_p\widetilde{u_j''\theta}$) are to be modelled (see the following subsections). It is noted, that the term $\overline{\tau}_{ij}^{\mu}\widetilde{S}_{ij}$ denoting the (viscous) dissipation function is omitted in the energy equation. Its contribution is negligible at low Mach numbers applied in the present work. In these equations the overbar ($\overline{\Phi}$) and the tilde ($\widetilde{\Phi}$) denote the standard (Reynolds) and the mass weighted (Favre) averages ($\widetilde{\Phi} \equiv \overline{\rho\Phi}/\overline{\rho}$), respectively. The temperature dependence on viscosity μ and heat conductivity λ is defined via a power-law formulation, while Prandtl number Pr and specific heat at constant pressure C_p were kept constant.

$$\overline{\mu} = \mu_{ref}\left(\frac{\widetilde{\Theta}}{\Theta_{ref}}\right)^{0.71} \quad ; \quad \overline{\lambda} = \lambda_{ref}\left(\frac{\widetilde{\Theta}}{\Theta_{ref}}\right)^{0.71} \tag{4}$$

Density is evaluated from the equation for ideal gas $\overline{\rho} = \overline{P}/(R\widetilde{\Theta})$, with R denoting the universal gas constant.

Turbulence Model

The present near-wall, second-moment closure model implies the solution of model transport equation for the Reynolds stress tensor $\widetilde{u_i''u_j''}$ (Eq. 2) and the equation governing a new scale-supplying variable, referred to as the 'homogeneous dissipation rate' ε^h (see Fig. 1), Jakirlic and Hanjalic (2002):

$$\frac{\partial(\overline{\rho}\widetilde{U}_k\widetilde{u_i''u_j''})}{\partial x_k} = \frac{\partial}{\partial x_k}\left[\left(\frac{1}{2}\overline{\mu}\delta_{kl} + C_s\overline{\rho}\frac{\widetilde{k}}{\varepsilon^h}\widetilde{u_k''u_l''}\right)\frac{\partial\widetilde{u_i''u_j''}}{\partial x_l}\right] + \overline{\rho}(\mathscr{P}_{ij} - \varepsilon_{ij}^h + \Phi_{ij,1} + \Phi_{ij,2} + \Phi_{ij}^w) \tag{5}$$

$$\frac{\partial(\overline{\rho}\widetilde{U}_k\varepsilon^h)}{\partial x_k} = \frac{\partial}{\partial x_k}\left[\left(\frac{1}{2}\overline{\mu}\delta_{kl} + C_\varepsilon\overline{\rho}\frac{\widetilde{k}}{\varepsilon^h}\widetilde{u_k''u_l''}\right)\frac{\partial\varepsilon^h}{\partial x_l}\right] + \overline{\rho}(C_{\varepsilon,1}\mathscr{P}_k - C_{\varepsilon,2}f_\varepsilon\tilde{\varepsilon}^h)\frac{\varepsilon^h}{\tilde{k}} + C_{\varepsilon,3}\overline{\mu}\frac{\tilde{k}}{\varepsilon^h}\widetilde{u_j''u_k''}\frac{\partial^2\widetilde{U}_i}{\partial x_j\partial x_l}\frac{\partial^2\widetilde{U}_i}{\partial x_k\partial x_l} \tag{6}$$

with $\mathscr{P}_{ij} = -\widetilde{u_i''u_k''}\partial\widetilde{U}_j/\partial x_k - \widetilde{u_j''u_k''}\partial\widetilde{U}_i/\partial x_k$ and $\mathscr{P}_k = 0.5\mathscr{P}_{ii}$ representing the stress production term and the production rate of the kinetic energy of turbulence respectively and $\tilde{\varepsilon}^h = \varepsilon^h - (\partial\tilde{k}^{1/2}/\partial x_l)^2$.

The quantity ε^h differs from the conventional dissipation rate ε ($= \varepsilon^h + \mathscr{D}_k^{\nu}/2$) by a non-homogeneous part, which is active only in the immediate wall vicinity up to $y^+ \approx 20$, Fig. 1. This 'inhomogeneous' part corresponds exactly to one half of the molecular diffusion of the kinetic energy of turbulence ($\mathscr{D}_k^{\nu} = \nu\partial^2\tilde{k}/\partial x_l\partial x_l$, Fig. 1) and, thus, it needs no modelling. Such an approach offers a number of convenient advantages: the dissipation equation (6) retains the same basic form, the proper near-wall behaviour of ε is recovered without any additional terms, and the correct asymptotic behaviour of the stress dissipation components $\varepsilon_{ij} = \varepsilon_{ij}^h + \mathscr{D}_{ij}^{\nu}/2$ ($\mathscr{D}_{ij}^{\nu} = \nu\partial^2\widetilde{u_i''u_j''}/\partial x_l\partial x_l$) when a solid wall is approached is fulfilled automatically without necessity for any wall geometry-related parameter.

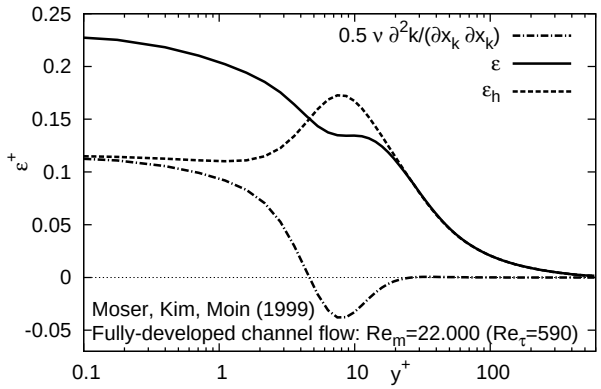

FIGURE 1. Total viscous dissipation rate ε split into the homogeneous part ε_h and the inhomogeneous part $0.5\nu(\partial^2 k/\partial x_k \partial x_k)$

The model employs the quadratic formulation of the pressure strain term:

$$\Phi_{ij,1} = -\varepsilon\left[C_1 a_{ij} + C_1'\left(a_{ik}a_{jk} - \frac{1}{3}\delta_{ij}A_2\right)\right] \tag{7}$$

$$\Phi_{ij,2} = C_3 k\widetilde{S}_{ij} + C_4 k\left(a_{ip}\widetilde{S}_{pj} + a_{jp}\widetilde{S}_{pi} - \frac{2}{3}a_{pq}\widetilde{S}_{pq}\delta_{ij}\right) + C_5 k\left(a_{ip}\widetilde{W}_{pj} + a_{jp}\widetilde{W}_{pi}\right) - C_2' a_{ij}\mathscr{P}_k \tag{8}$$

The mean vorticity tensor is given by $\widetilde{W}_{ij} = 0.5(\partial\widetilde{U}_i/\partial x_j - \partial\widetilde{U}_j/\partial x_i)$. $a_{ij} = \widetilde{u_i''u_j''}/\tilde{k} - 2\delta_{ij}/3$, $A_2 = a_{ij}a_{ji}$, $A_3 = a_{ij}a_{jk}a_{ki}$, $A = 1 - 9(A_2 - A_3)/8$, $e_{ij} = \varepsilon_{ij}^h/\varepsilon^h - 2\delta_{ij}/3$, $E_2 = e_{ij}e_{ji}$, $E_3 = e_{ij}e_{jk}e_{ki}$, $E = 1 - 9(E_2 - E_3)/8$ and $Re_t = \tilde{k}^2/(\nu(\varepsilon^h)^2)$ are the Reynolds stress and stress-dissipation anisotropy tensors and their invariants and turbulence Reynolds number respectively. The constitutive part of the pressure-strain model is the Gibson and Launder (1978) formulation of the wall reflection term Φ_{ij}^w:

$$\Phi_{ij}^w = C_1^w f_w \frac{\varepsilon^h}{\widetilde{k}}\left(\widetilde{u_k''u_m''}n_k n_m\delta_{ij} - \frac{3}{2}\widetilde{u_i''u_k''}n_k n_j - \frac{3}{2}\widetilde{u_k''u_j''}n_k n_i\right) + C_2^w f_w \frac{\varepsilon^h}{\widetilde{k}}\left(\Phi_{km,2}^{IP}n_k n_m\delta_{ij} - \frac{3}{2}\Phi_{ik,2}^{IP}n_k n_j - \frac{3}{2}\Phi_{kj,2}^{IP}n_k n_i\right) \tag{9}$$

The linear *isotropization-of-production* (IP, Launder et al., 1975) formulation of the rapid pressure-strain model $\Phi_{ij,2}^{IP} = -C_2(\mathscr{P}_{ij} - 2\mathscr{P}_k\delta_{ij}/3)$ ($C_2 = 0.8A^{1/2}$) was retained in the term modelling the wall influence on the rapid pressure scrambling process.

The stress dissipation tensor was modelled by using the following anisotropic formulation

$$\varepsilon_{ij}^h = f_s\frac{\widetilde{u_i''u_j''}}{\tilde{k}}\varepsilon^h + (1 - f_s)\frac{2}{3}\delta_{ij}\varepsilon^h \tag{10}$$

with $f_s = 1 - \sqrt{A}E^2$.

Besides performing the calibration of the model coefficients by computing appropriate reference flow geometries, whereby the results obtained are accommodated to available experimental or DNS data, coefficients determination is supported by their *a priori* evaluation by using the available DNS database of a fully-developed channel flow, Jakirlic (2004). E.g., the functional dependency of the coefficient C_1' in the nonlinear part of the slow term (Eq. 7) is obtained by such a method, Fig. 2. For each combination of two different components (e.g., $ij = 11$ and $ij = 22$; other combinations can also be used) of the slow term, the model formulation for $\Phi_{ij,1}$ (Eq. 7) can be written as a system of two equations with two unknowns C_1 and C_1'. The input data for all variables (also for $\Phi_{ij,1}$) were taken from the DNS database of a fully-developed channel flow. The coefficients in the rapid part $\Phi_{ij,2}$ can be evaluated by using the same method (this time a system of three equations - e.g., $ij = 11$, $ij = 22$ and $ij = 12$ - with three unknowns C_2', C_4 and C_5 was solved; C_3 coefficient has been taken as known, e.g., $C_3 = 0.8 - 0.65\sqrt{A_2}$ in the Speziale, Sarkar and Gatski (SSG, 1991) model, Fig. 2). The C_2' profiles obtained from the DNS database of the plane channel flow for $Re_\tau = 180$ (Moser et al., 1999) exhibit values between -0.2 and 0.2, missing by far the positive value in, e.g., the SSG model ($C_{2,SSG}' = 0.9$), whereas the evaluated profiles of the coefficients C_4 and C_5 exhibit the values agreeing well with the SSG proposal. The appropriate value and even the sign of the coefficient C_2' remain to be clarified. Because of this uncertainty its value was set to zero in the present work, i.e. the linear model for the rapid part was applied.

The wall reflection term model was made wall-normal free by introducing a unit vector pointing into the direction of the non-homogeneity of the turbulence field, in line with the proposal of Gerolymos and Vallet (2002): $\mathbf{n} = \nabla l/|\nabla l|$. Hereby, a modified length scale $l = A\tilde{k}^{3/2}/\varepsilon^h$ was adopted as a parameter reflecting the turbulence non-homogeneity. As illustration, the contours of the n_i - components obtained using the DNS database of the backward-facing step flow (Le et al., 1997) are displayed in Figs. 3.

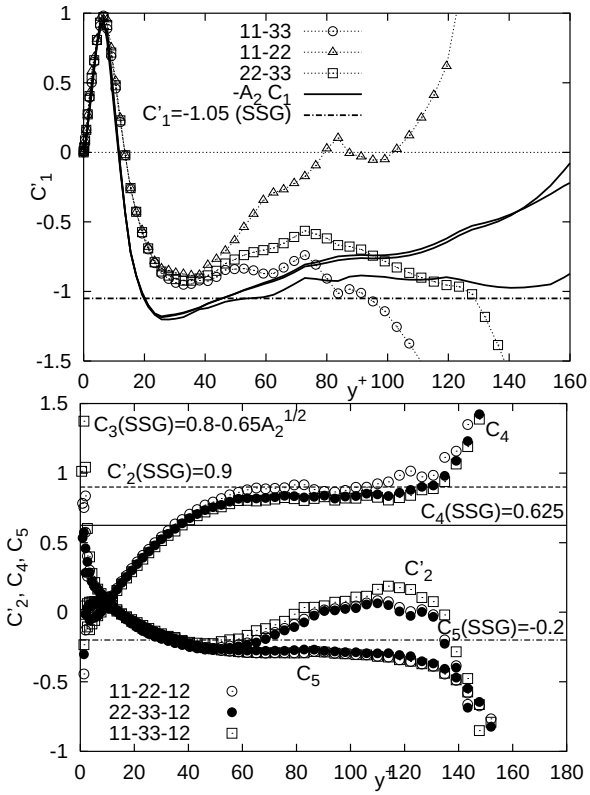

FIGURE 2. Profiles of C_1', C_2', C_4 and C_5 in the fully developed channel flow obtained by application of an *a priori* method on Eqs. (7) and (8) (Jakirlic, 2004)

The model coefficients are given as follows:

$$C_1 = 2.5AF^{1/4}f + \sqrt{A}E^2,\ \ F = \min\{0.6; A_2\}$$
$$f = \min\left\{(Re_t/150)^{3/2}; 1\right\},\ \ C_1' = -\max\{0.7A_2; 0.5\}C_1$$
$$C_3 = 1.067A^{1/2},\ \ C_4 = -C_5 = 0.8A^{1/2},\ \ C_2' = 0$$
$$C_1^w = \max(0.9 - 1.75AF^{1/4}f; 0.3),\ \ C_2^w = \min(A; 0.3)$$
$$C_s = 0.22,\ \ C_{\varepsilon,1} = 1.44,\ \ C_{\varepsilon,2} = 1.8,\ \ C_{\varepsilon,3} = 0.3,\ \ C_\varepsilon = 0.18$$

Prior to the computations using complete model, the performances of the present model for the stress dissipation were checked *a priori* using the DNS database of some related wall-bounded flows (flow in a fully-developed channel, DNS by Moser et al., 1999), Fig. 4-upper. The model captured the dissipation anisotropy in good agreement with the DNS data. The results obtained with the Rotta's isotropic model ($\varepsilon_{ij} = 2\varepsilon\delta_{ij}/3 \Rightarrow \varepsilon_{11} = \varepsilon_{22} = \varepsilon_{33} = 2\varepsilon/3$; $\varepsilon_{12} = \varepsilon_{13} = \varepsilon_{23} = 0$) are also shown for comparison. It is clearly seen, that the anisotropies of the dissipation correlation are not only pronounced in the immediate wall vicinity, but they also affect the core flow. This feature is beyond the reach of the Rotta's proposal. The effects of the non-

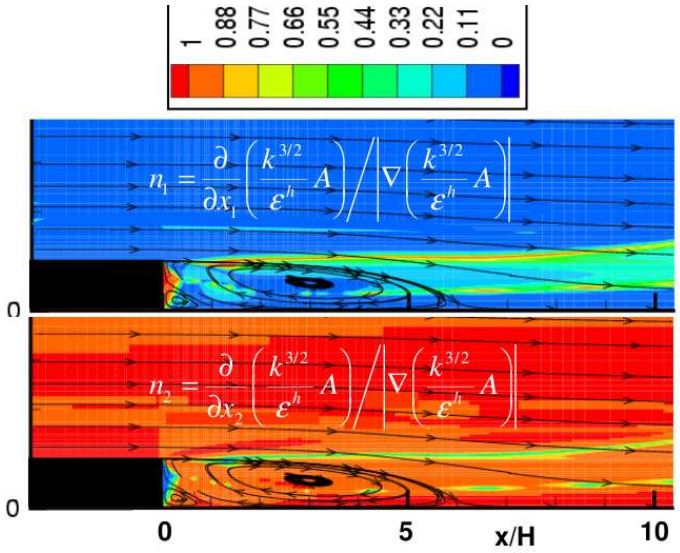

FIGURE 3. Contours of the n_1 (upper) and n_2 (lower) components of the unit vector n_i in the flow over a backward-facing step

linear addition on the redistribution among the Reynolds stress components are unambiguous, as illustrated in the flow over a backward-facing step (DNS by Le et al., 1997), Fig. 4-lower. Streamwise position $x/H = 4$ corresponds to the separation bubble.

Figs. 5 displays the Reynolds stress components and terms in the budget of the kinetic energy of turbulence equation (Production rate $\mathscr{P}_k$, 'homogeneous' (ε^h) and non-homogeneous $0.5\mathscr{D}_k$ dissipation rates) obtained by using the complete set of the model equations exhibiting excellent agreement with the reference DNS data of Kasagi and Iida (1999).

The applied turbulence model for the variable fluid property (i.e. compressible) cases is a straight-forward adaptation of the incompressible version of the turbulence model. No additional modelling effort was spent to adequately modified the turbulent diffusion $\mathscr{D}_{ij}^t$ and pressure-strain correlation Φ_{ij}. The additional terms in the Reynolds-stress transport equation, arising from the Favre averaging, the so-called pressure dilatation correlation and mass flux coupling, were not taken into consideration. The pressure dilatation correlation term requires information about pressure fluctuation p' which are not available. The mass flux coupling term contains velocity fluctuation u''. It might be evaluated by additional model transport equations, leading eventually to the high computational costs, or by an algebraic model, e.g. Huang et al. (1995). Neglecting its influence is a common assumption in relevant compressible flows.

Heat flux modelling A model describing the unknown turbulent heat fluxes is required when solving the turbulent

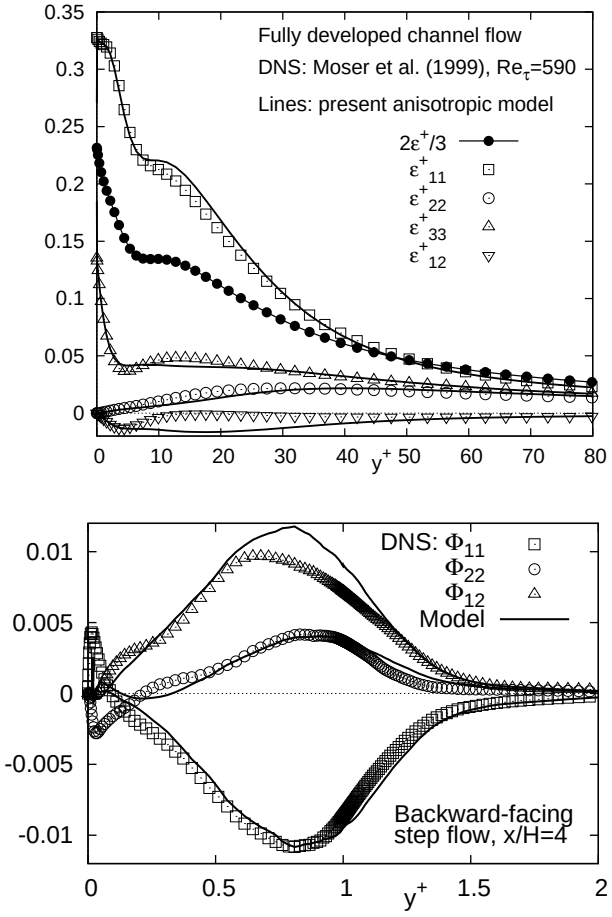

FIGURE 4. Stress dissipation components obtained by the present anisotropic model (Eq. 10) and pressure-strain-term components defined by Eqs. (7-9)

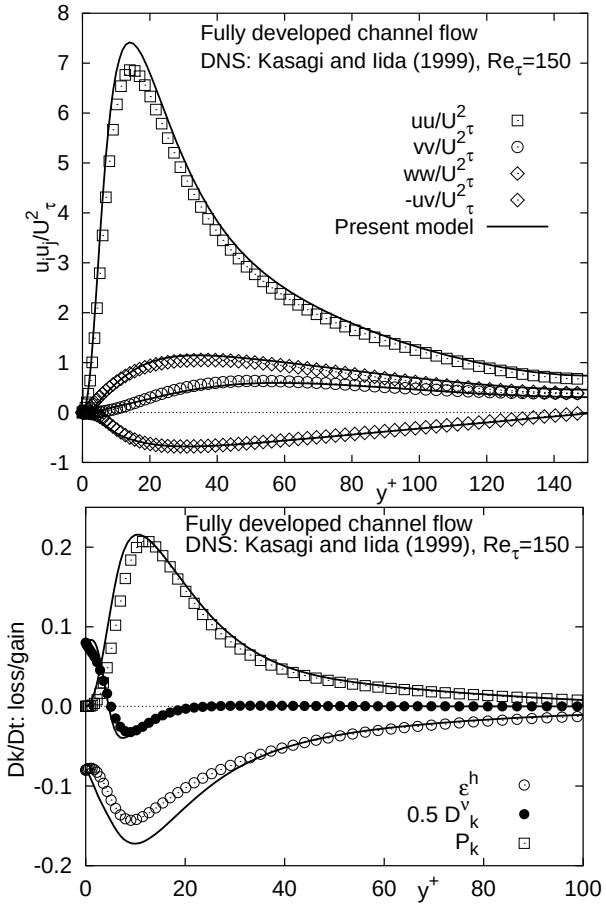

FIGURE 5. Reynolds stress components (upper), terms in the budget of the equation for the kinetic energy of turbulence (lower) in a channel flow with constant fluid properties (DNS: Kasagi and Iida, 1999) obtained with the present turbulence model

energy equation. A common approach is the prescription of a constant Prandtl number in the framework of the simple gradient diffusion hypothesis (SGDH) or the general gradient diffusion hypothesis (GGDH), the latter employing the Reynolds stress tensor and turbulent time scale in the diffusion coefficient. More sophisticated models solve additional differential equations either for temperature variance $\widetilde{\theta^2}$ and scalar dissipation ε_θ or directly for the turbulent heat fluxes $\widetilde{u_i''\theta}$:

$$\frac{D(\overline{\rho}\widetilde{u_i''\theta})}{Dt} = \mathscr{D}^{\nu}_{i\theta} + \mathscr{D}^{t}_{i\theta} + \overline{\rho}\,\mathscr{P}_{i\theta} + \overline{\rho}\Phi_{i\theta} - \overline{\rho}\varepsilon_{i\theta} \qquad (11)$$

with $\mathscr{P}_{i\theta} = -\widetilde{u_i''u_j''}\partial\widetilde{\Theta}/\partial x_j - \widetilde{u_j''\theta}\partial\widetilde{U}_i/\partial x_j$. The latter model group is in the focus of the present work. Three turbulent heat flux models were applied presently, differing mainly in the formulation of the pressure-temperature gradient term $\Phi_{i\theta}$ (Eq. 13).

In conjunction with the differential Reynolds-stress turbulence model described in the section before, only the near-wall heat transfer models were taken into account.

The basic model, denoted as model **I** throughout the work, is the proposal of Lai and So (1990). The corresponding model coefficients are given as follows:

$$C_\theta = 0.11,\ C_{\theta 11} = 3.0,\ C_{\theta 31} = 0.4$$
$$C_{\theta,w} = 0.75,\ f_\theta = \exp[-(Re_t/80)^2]$$

All other coefficients in Eq. (13) take the value zero.

Model **II** is an extension of the basic model to account for the mean scalar gradient, a proposal introduced by Jones (1992) in the context of a high Reynolds number scalar transport model: $C_{\theta 22} = 0.25$. All other coefficients are same as in the model **I**.

Model **III** is a recent development of Seki et al. (2003) being characterized by a very complex definition of the pressure-

temperature-gradient correlation. Its coefficients are formulated as follows:

$$C_\theta = 0.11,\ C_{\theta 11} = 2.9(1-0.74\exp(-Re_t/100)+0.55 f_\varepsilon)$$
$$C_{\theta 12} = -0.5,\ C_{\theta 21} = C_{\theta 22}/3,\ C_{\theta 22} = 0.01\sqrt{A},\ C_{\theta 31} = 0.1$$
$$C_{\theta 32} = 0.0035,\ C_{\theta 33} = 0.1,\ C_{\theta 34} = 0.01,\ C_{\theta 41} = 0.188$$
$$C_{\theta 42} = -0.102,\ C_{\theta 43} = 0.1,\ C_{\theta,w} = 0.75,\ f_\theta = \exp(-y^+/15)$$
$$f_\varepsilon = \min\left(1, Pr^{1/3}\right)\exp(-Re_t/2000)$$

This model was hitherto only *a priori* tested in a term-by-term manner. This will be the first application of such a low Reynolds number model in conjunction with the previously described near-wall, second-moment closure model for the combined momentum and heat transfer under conditions of variable fluid properties.

While the production term $\mathscr{P}_{i\theta}$ (Eq. 11) do not need any modelling, the viscous diffusion $\mathscr{D}^{\nu}_{i\theta}$ is modelled in the way fulfilling the near wall behaviour.

$$D^{\nu}_{i\theta} = \frac{\partial}{\partial x_j}\left[\overline{\eta}\frac{\partial \widetilde{u_i''\theta}}{\partial x_j} + \frac{\overline{\rho}\,\overline{a}-\overline{\eta}}{n_i+2} n_k \frac{\partial \widetilde{u_k''\theta}}{\partial x_j}\right] \tag{12}$$

The model formulation of the pressure-temperature gradient term consisting all three afore-mentioned model proposals reads:

$$\begin{aligned}
\Phi_{i\theta} = &\left(-C_{\theta 11}\frac{\varepsilon}{k}\widetilde{u_i''\theta} - C_{\theta 12} a_{ij}\frac{\varepsilon}{k}\widetilde{u_j''\theta}\right)(1-f_\theta)\\
&+C_{\theta 21} k\frac{\partial \widetilde{\Theta}}{\partial x_i} - C_{\Theta 22} a_{ij} k\frac{\partial \widetilde{\Theta}}{\partial x_j}\\
&+C_{\theta 31}\widetilde{u_j''\theta}\frac{\partial \widetilde{U}_i}{\partial x_j} + C_{\theta 32}\widetilde{u_j''\theta}\frac{\partial \widetilde{U}_j}{\partial x_i}\\
&+C_{\theta 33}\widetilde{u_i''u_j''u_k''\theta}\frac{1}{k}\frac{\partial \widetilde{U}_j}{\partial x_k}\\
&+C_{\theta 34}\left(\widetilde{u_i''u_k''u_j''\theta} + \widetilde{u_j''u_k''u_i''\theta}\right)\frac{1}{k}\frac{\partial \widetilde{U}_j}{\partial x_k}\\
&+C_{\theta 41}\frac{k^2}{\varepsilon}\frac{\partial \widetilde{U}_i}{\partial x_j}\frac{\partial \widetilde{\Theta}}{\partial x_j}\\
&+C_{\theta 42}\widetilde{u_i''u_j''}\frac{k}{\varepsilon}\frac{\partial \widetilde{U}_j}{\partial x_k}\frac{\partial \widetilde{\Theta}}{\partial x_k}\\
&+C_{\theta 43}\frac{k}{\varepsilon}\frac{\partial \widetilde{U}_j}{\partial x_k}\left(\widetilde{u_i''u_k''}\frac{\partial \widetilde{\Theta}}{\partial x_j} + \widetilde{u_k''u_j''}\frac{\partial \widetilde{\Theta}}{\partial x_i}\right)\\
&+f_\theta\left(C_{\theta 11}\frac{\varepsilon}{k}\widetilde{u_i''\theta} - \frac{\varepsilon}{k}\widetilde{u_k''\theta} n_k n_i\right)\\
&+C_{\theta,w}\frac{\varepsilon}{k}\widetilde{u_k''\theta} n_k n_i \frac{k^{3/2}}{\varepsilon y}
\end{aligned} \tag{13}$$

The model for the turbulent transport $\mathscr{D}^{t}_{i\theta}$ is the gradient diffusion model due to Daly and Harlow (1970)

$$\mathscr{D}^{t}_{i\theta} = \frac{\partial}{\partial x_k}\left(C_\theta \overline{\rho}\frac{k}{\varepsilon}\widetilde{u_k''u_j''}\frac{\partial \widetilde{u_i''\theta}}{\partial x_j}\right) \tag{14}$$

Contrary to the high Reynolds number scalar transport models, the viscous dissipation should not be neglected. The dissipation model adopted in the present work is the proposal of Lai and So (1990):

$$\varepsilon_{i\theta} = 0.5 f_\theta\left(1+\frac{1}{Pr}\right)\frac{\varepsilon}{k}\left(\widetilde{u_i''\theta} + \widetilde{u_k''\theta} n_k n_i\right) \tag{15}$$

Numerical method All computations were performed by an own in-house computer code based on the Finite Volume numerical method (2nd order) for solving RANS-equations on the orthogonal computational grids. The closest-to-the-wall grid point was located at $y^+ \leq 0.5$. In order to account for the compressibility effects an appropriately modified SIMPLE pressure-correction method in conjunction with the collocated variable arrangement was used.

FLOW CONFIGURATIONS CONSIDERED

Two channel flows in conjunction with the scalar transport under conditions of constant (DNS: Kasagi and Iida, 1999) and variable fluid properties (LES: Wang and Pletcher, 1996) were considered, focusing on the configuration with a temperature gradient between the upper and lower walls, Fig. 6. In the case a) the ratio of the wall temperatures is slightly higher than unity, providing the temperature can be treated as a passive scalar, Kasagi and Iida (1999). In the case b) the ratio of the upper wall temperature to the lower wall temperature was varied up to 3, Wang and Pletcher (1996). In this case the effects of the variable fluid properties must be accounted for.

Schematic of the backward-facing step flow configuration indicating the domain of interest is displayed in Fig. 7. The flow Reynolds number based on the step height and the upstream centerline velocity is $Re_H = 5540$ ($H = 0.041m$). The upstream conditions correspond to fully-developed flow in a channel of height $2h$ (inflow was generated by performing precursor channel flow calculations) providing the expansion ratio of $ER = 1.5$. The bottom wall downstream of the step was heated by a uniformly supplied heat flux, the latter representing the thermal boundary conditions. Three cases with increasing heat flux ($q_w = 1$, 2 and 3 kW/m^2; reference LES by Avancha, 2001, and Avancha and Pletcher, 2002) were computed in addition to the isothermal flow (Exp.: Kasagi and Matsunaga, 1995). All other flow

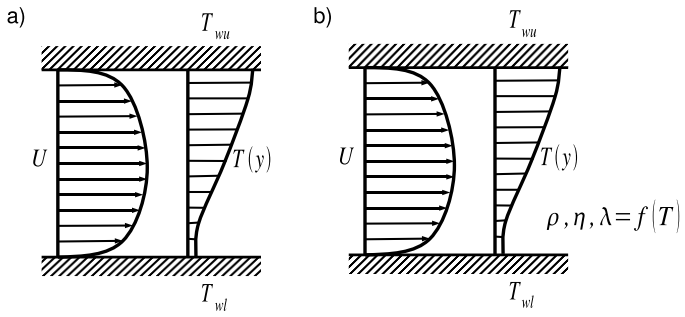

FIGURE 6. Test cases considered: a) with constant fluid properties and b) with variable fluid properties

and fluid properties were adopted from the work of Avancha and Pletcher: $U = 2.063\,m/s$, $\Theta_{ref} = 293\,K$, $\rho_{ref} = 1.194\,kg/m^3$, $\lambda_{ref} = 0.2574\,W/(mK)$, $\nu_{ref} = \mu_{ref}/\rho_{ref} = 1.527 \times 10^{-5} m^2/s$, $Pr = 0.71$ and $C_p = 1006\,J/(kgK)$.

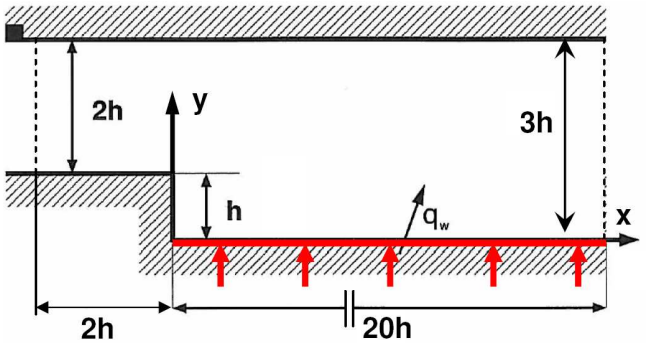

FIGURE 7. Schematic of flow configuration considered

The third flow configuration considered in this work representing a vertical circular tube with air flowing in upward direction was experimentally investigated by Shehata and McEligot (1998), Fig. 8. After a portion of a fully-developed pipe flow (length = $4D$, with D being the pipe diameter) with constant wall temperature Θ_w the air enters a $30D$-long pipe subjected to intensive heating (with negligible buoyancy effects). The thermal boundary conditions correspond to a constant heat flux. Three different heating rates were considered $q_i^+ = 0.0018$, 0.0035 and 0.0045. In the latter case for which the DNS database obtained by Satake et al. (2000) and Bae et al. (2006) was also available, some laminarization phenomena have been observed. Due to sake of brevity, only this flow will be considered here.

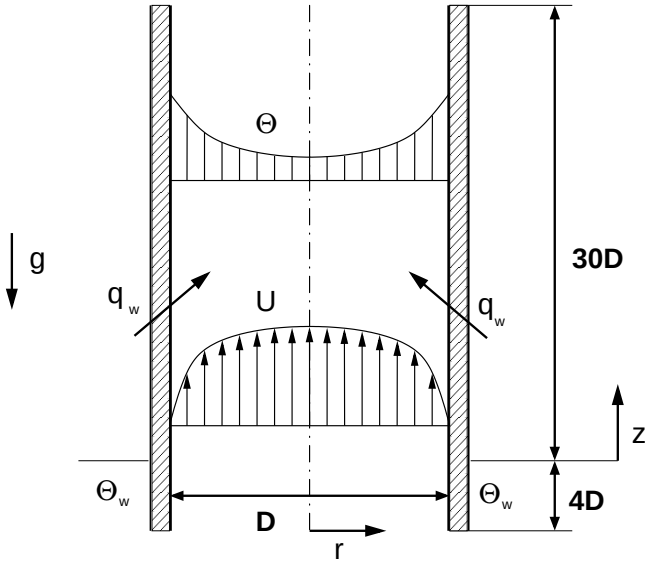

FIGURE 8. Flow configuration considered

RESULTS AND DISCUSSION

Results obtained by applying the present $\overline{\rho}\widetilde{u_i'' u_j''} - \varepsilon^h$ turbulence model (denoted by RSM throughout the results section) to the three selected flow configurations featured by severe property variations due to large temperature gradients being the consequence of a strong wall heating are presented and discussed along with the available reference experimental and numerical data in the following sections.

Fully-developed channel flow

Channel flow with constant flow properties The periodic inlet/outlet boundary conditions were applied here in order to provide the conditions of a fully-developed flow. Before starting with the model calculations of the conjugate momentum and heat transfer under the conditions of property variations, the implemented heat flux models were tested in a channel flow with constant-fluid properties (passive scalar transport) at bulk Reynolds number $Re_m = 4560$, for which the reference DNS has been performed by Iida and Kasagi (1999). The corresponding Reynolds stress components, production and dissipation rates of the turbulent kinetic energy are displayed in Fig. 5. The thermal boundary conditions correspond to a constant wall temperature. The ratio of the bottom wall temperature to the temperature of the top wall is chosen small enough providing the velocity field being not affected. The equations for the mean temperature, scalar fluxes and dissipation rate were solved, whereas the velocity and Reynolds stress fields were taken from the DNS database. All heat flux models predicted the mean temperature profile in reasonable agreement with the DNS results, Fig. 9, with a certain underprediction being mostly pertinent when using the model *II*.

A more differentiated behaviour can be observed when analyzing the heat fluxes. All models predicted well the $\widetilde{v''\theta}$ component (being the only reminding heat flux component in the energy equation 3, simplified under conditions of fully-developed flow), unlike the streamwise heat flux $\widetilde{u''\theta}$, which could be correctly reproduced only by the model *III*. Obviously that the non-linear description of the interaction between the heat flux and the turbulent Reynolds stresses in the expression for $\Phi_{i\theta}$, including both the mean velocity and mean temperature gradients, contributed strongly to the correct capturing of the component $\widetilde{u''\theta}$. The $\widetilde{u''\theta}$ profiles obtained with the models *I* and *II* follow the same tendency as the DNS result, but their intensities exhibit a severe underprediction.

Channel flow with variable flow properties The applicability of the adopted model for the heat transfer problems with the velocity and Reynolds stress fields being strongly affected by the thermal field is further tested in a low Reynolds number ($Re_m = 5400$) fully-developed channel flow exhibiting large density and viscosity gradients due to strong heating. The LES computation of Wang and Pletcher (1996) served here as reference. The thermal boundary conditions are analog to those in the case a) (constant fluid property flow), but with a much higher difference between the temperatures of the top and bottom wall. As the reference case, the temperature ratio $\Theta_{wu}/\Theta_{wl} = 3.0$ is selected. The influence of temperature on density ρ, viscosity η and thermal diffusivity λ is taken into consideration. The hot wall is located at $y/h = 1$, while the position of the cold wall corresponds to $y/h = -1$. Fig. 10-upper displays the mass flow rate $\overline{\rho}\widetilde{U}$ across the channel. The temperature gradient and consequently the density variation in the channel cross-section causes the asymmetric velocity profile, unlike in the constant density flows. The basic profile is obtained in reasonable agreement with the DNS data. The slopes of the mass flow rate profile at both the bottom and top walls are well captured. However, the analysis of the position of its maximum value (position with the zero gradient of the mass flow rate) reveals important differences. Whereas the DNS profile exhibits its maximum close to the bottom, that is 'cold' wall, the location of the maximum value of $\overline{\rho}\widetilde{U}$ computed by both models adopted is shifted towards the channel center. The origin of this deviation is to be sought in the temperature and density variation, Fig. 11. Closer agreement reveals the comparison of the mean axial velocity component obtained by the model computations, Fig. 10-lower. The DNS results exhibit an almost symmetric profile. One notes different wall shear stresses at lower and upper walls. Despite the generally well predicted behaviour of the temperature field, exhibiting a positive gradient across the entire cross-section with its highest value in the wall regions, the temperature of the upper ('hot') wall exhibits a certain overprediction (pertinent to model *I*). The value of $\widetilde{\Theta}_{wu}/\widetilde{\Theta}_0 = 1.6$ obtained by the model is compared with the

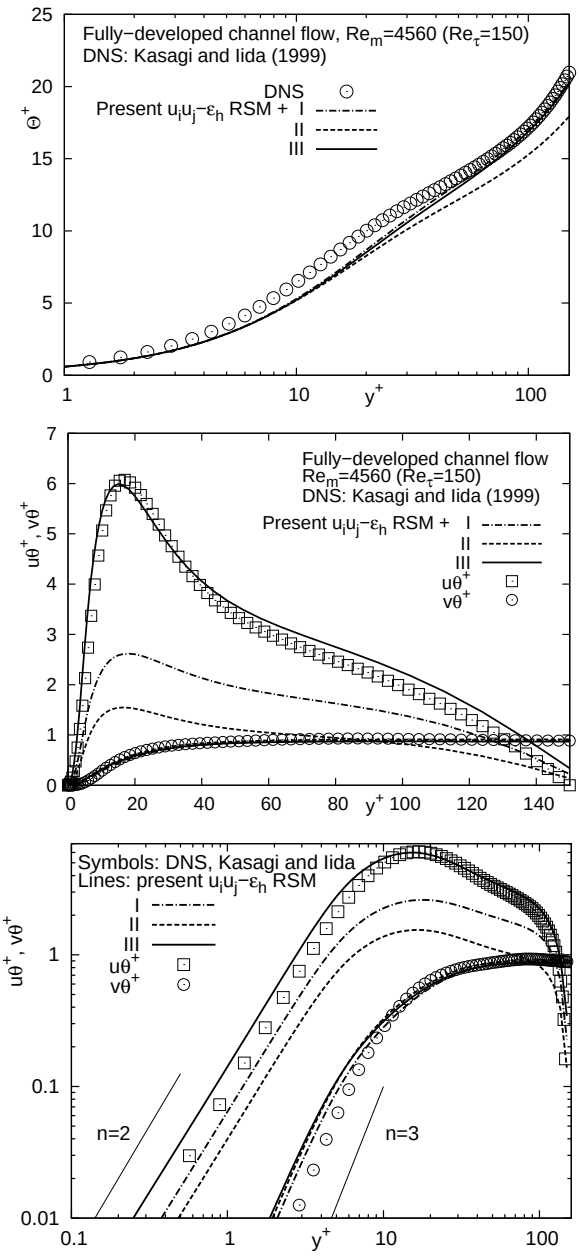

FIGURE 9. Mean temperature Θ^+ and heat flux components $\widetilde{u''\theta}^+$ and $\widetilde{v''\theta}^+$ in a channel flow with constant fluid properties

LES value of 1.5. Since the wall temperatures are fixed through the boundary conditions applied, this overprediction implies actually the underprediction of the centerline temperature $\widetilde{\Theta}_0$, causing finally a steeper temperature gradient compared with the LES results. The previously described deviations of the mass flow rate (Fig. 10) and the mean temperature profile (Fig. 11) rep-

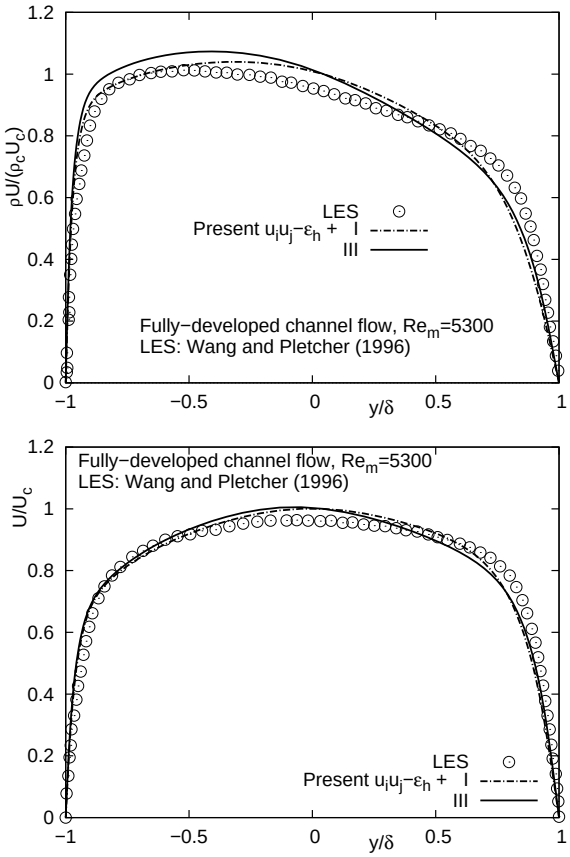

FIGURE 10. Mass flow rate $(\overline{\rho}\widetilde{U})/(\overline{\rho}_0\widetilde{U}_0)$ (upper) and axial velocity $\widetilde{U}/\widetilde{U}_0$ (lower)

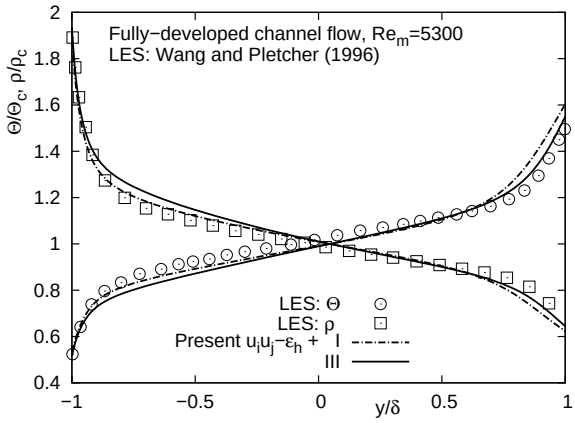

FIGURE 11. Temperature and density profiles (normalized by appropriate centerline values)

resent the main cause for a poor prediction of the streamwise heat flux component (Fig. 12 upper). The production rate of this flux component ($\mathscr{P}_{1\theta}$) and the component itself take zero values at the location coinciding with the zero velocity gradient (velocity maximum) and zero shear stress component $\widetilde{u''v''}$ (not shown here). The heat flux model *I* underestimates substantially the intensity of $\widetilde{u''\theta}$ in the vicinity of the both walls. Furthermore, the modelled flux component $\widetilde{u''\theta}$ is characterized by a completely flat profile (zero gradient) over a large portion of the lower channel half in contrast to the LES result, which exhibits a substantial gradient. Much closer agreement, despite certain underprediction of the peak values in the vicinity of both walls, was documented when using the model *III*. The heat flux component $\widetilde{v''\theta}$ (Fig. 12 lower) is regarded as the most important component with respect to the temperature profile prediction (Fig. 11), since only this flux enters the equation governing the temperature field in a fully-developed channel flow. Global behaviour of this component is well predicted by both models used. Some differences between the LES and RANS calculations pertinent to the model *I* can be observed in the near-wall regions. The non-linear model *III* exhibits very good agreement with the reference LES in the entire channel cross-section. Fig. 13 displays the streamwise and normal-to-the-wall Reynolds stress components u_{rms} and v_{rms}. The main characteristic of both profiles is their asymmetric shape. Whereas the streamwise component agrees reasonably well with the LES data, the normal component shows a certain deviation in the lower channel half. The production rate $\mathscr{P}_{11}$ (due to the mean flow deformation) determines to a large extent the profile of the stress u_{rms}. The velocity gradient at the bottom wall is somewhat stronger compared to the upper wall (Fig. 10), resulting in a larger streamwise intensity in the immediate bottom-wall vicinity (compare the gradients of the streamwise turbulence intensity at both walls). However, the situation changes at the positions $y/h = -0.9$ and $y/h = 0.9$, leading to correspondingly higher peak value of u_{rms} in the upper channel half. The location of the minimum intensities obtained by both LES and RANS across the channel reflects completely the positions of the corresponding velocity maxima, Fig. 10 (lower). Because the production rate $\mathscr{P}_{22}$ (exact term) takes the zero value, the same analysis is not possible for the normal turbulence intensity v_{rms}. Its behaviour is entirely dependent on the turbulence model used.

Generally speaking, the non-linear pressure-temperature gradient term model (denoted by *III*) is superior to other models applied. Because of that, only this model is applied in the computations of the backward-facing step flow and laminarizing pipe flow.

Backward-facing step flow

Isothermal flow The comparison of the mean velocity field, Fig. 14, shows that the present RSM model yields the reattachment length of $x_r/H = 6.48$, in a very good agreement with

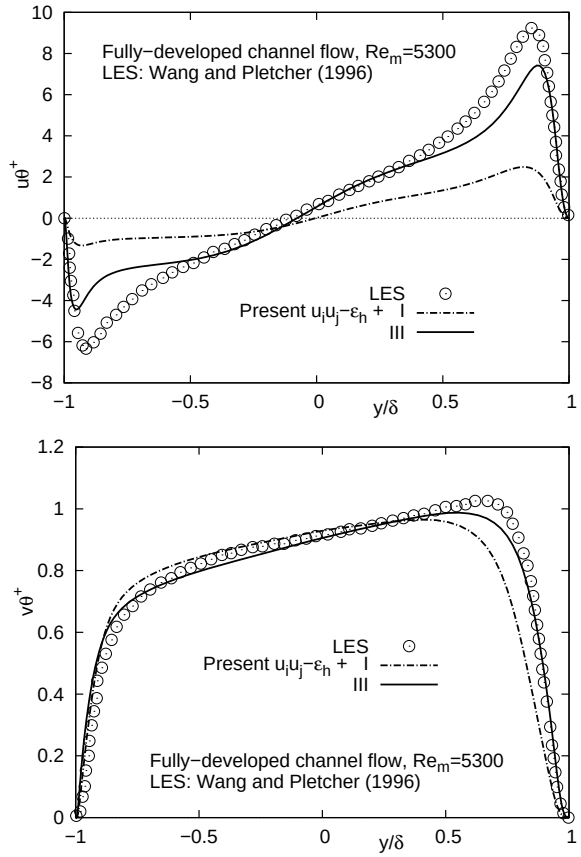

FIGURE 12. Heat flux components $\widetilde{u\theta}/q_w$ and $\widetilde{v\theta}/q_w$

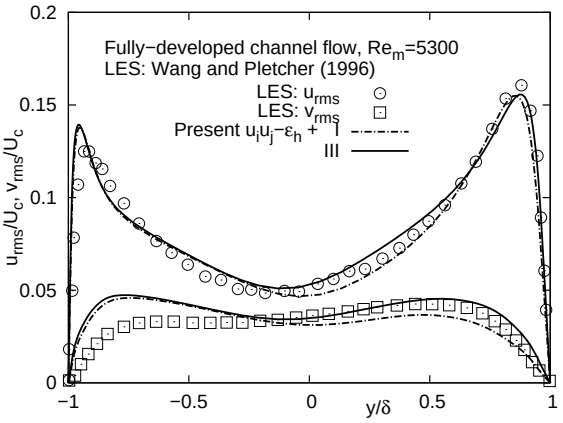

FIGURE 13. Turbulent stresses $u_{rms}/\widetilde{U}_0$ and $v_{rms}/\widetilde{U}_0$

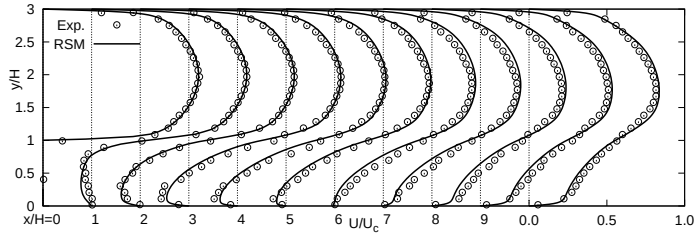

FIGURE 14. Evolution of the mean axial velocity profile - isothermal case

the experimental one $x_r/H = 6.51$. Furthermore, Fig. 14 displays excellent agreement between present computational results and experimental data in all characteristic regions of the backward-facing step configuration.

Cases with wall heating The calculations were performed for three different wall heat fluxes $q_w = 1$, 2 and $3\,kW/m^2$ (corresponding to the normalized heat flux levels - $Q_w = q_w/(\rho_{ref} C_p U_{ref} \Theta_{ref})$ - of 0.0014, 0.0028 and 0.0042). Fig. 15 depicts the mean axial velocity and mean temperature evolution for the case with the highest wall heat flux level $q_w = 3\,kW/m^2$. Direct comparison of the mean velocity field with the isothermal case (putting the profiles into the same diagram) reveals very weak influence of the strong temperature variation on the reattachment length (the same conclusion can be drawn from the C_f evolutions for all three heat flux levels, Fig. 16). The most important change compared to the isothermal case is visible in the region of the secondary recirculation and associated reattachment region. The influence of the strong temperature gradient (the wall temperature for the case with $q_w = 3\,kW/m^2$ takes here the values slightly below $1000\,K$, see e.g., Fig. 17) on the flow immediately after expansion is visible in all following diagrams.

The C_f evolutions displayed in Fig. 16 reveal a very interesting dependence on the heat flux level supplied. In order to make direct comparison between the reference LES and the present computational results the values on x-axis are normalized with the corresponding reattachment length. It should be noted that the reference LES results show some curious behaviour immediately after expansion, such as high positive values at the separation point $x/H = 0$, where, per definition, C_f should take zero value; accordingly, they should be handled with caution. Therefore, the results obtained by a Hybrid LES/RANS method (denoted by HLR), proposed recently by Jakirlic et al. (2009), are displayed in addition aiming at more reliable comparative assessment of the RSM predictions. The C_f developments are characterized by high negative peaks in the recirculation zone. The $q_w = 3kW/m^2$ case exhibit up to two times higher magnitude compared to the lowest heat flux ($q_w = 1kW/m^2$) case. The positive maximum value in the recovery region (an increase of 100% compared to the case with $q_w = 1kw/m^2$) increases with the heat

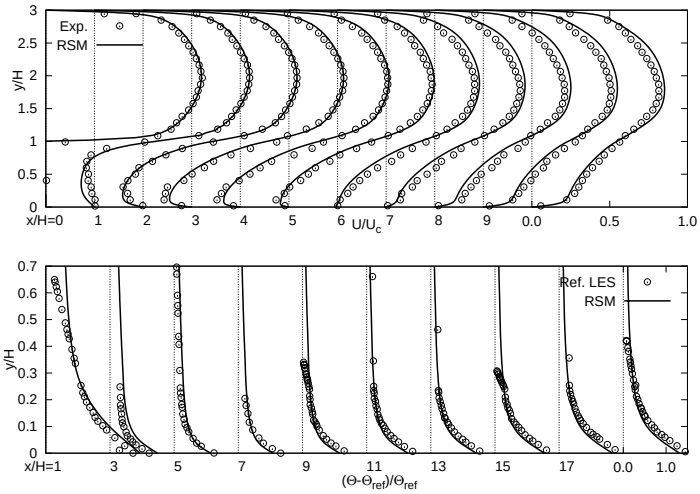

FIGURE 15. Evolution of the mean axial velocity and mean temperature profiles - $q_w = 3kW/m^2$

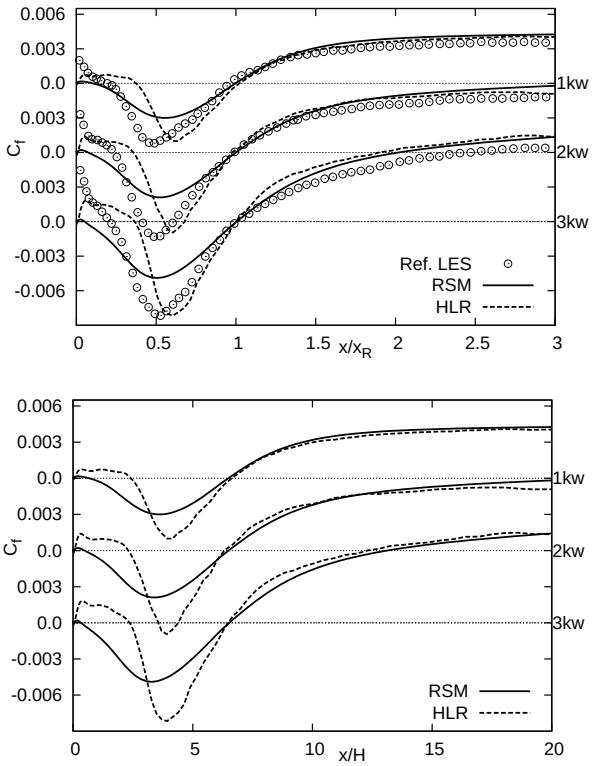

FIGURE 16. Friction coefficient evolution for all three cases with wall heating - $q_w = 1$, 2 and $3kW/m^2$

flux level increase. Such an outcome is pertinent to the intensification of the convective mixing within the separation bubble due to the strong heating. Although less intensive, an analogous acceleration occurs in the immediate wall vicinity within recovery region. As expected, the present RSM model underpredicts significantly the reference LES and the HLR results. The incapability of near-wall RANS models to correctly capture a strongly pronounced negative maximum of C_f pertinent to the separation bubble at such a low Reynolds number is well known, see e.g. Hanjalic and Jakirlic (1998). However, the C_f dependence on the heat flux in the recovery region was returned in very good agreement with both the reference LES and HLR results.

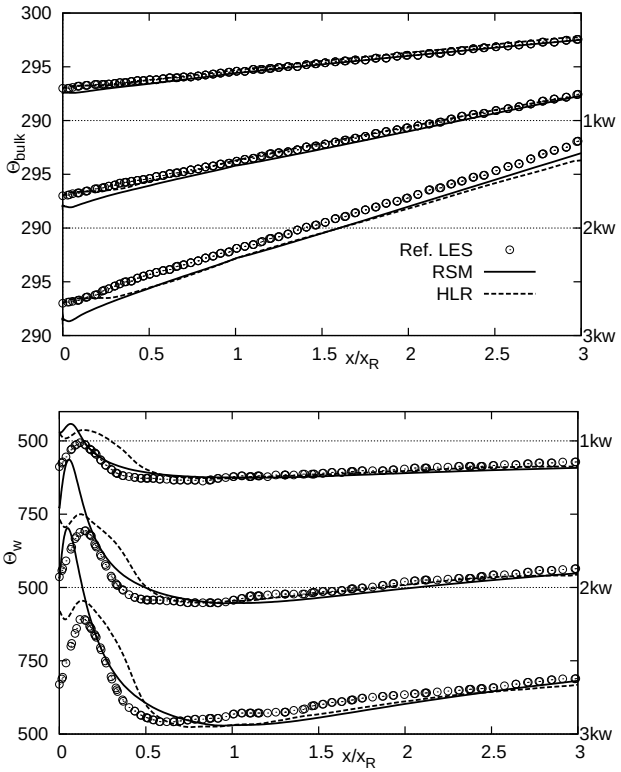

FIGURE 17. Bulk (upper) and wall (lower) temperature variation for all three cases with wall heating - $q_w = 1$, 2 and $3kW/m^2$

Both the bulk and the wall temperature variations agree well with the reference LES. Fig. 18 displays the variation of the coefficient of the dynamic viscosity. As expected, $\overline{\mu}$ reaches its maximum at the position coinciding with the secondary reattachment location, where the back-flow in the mean recirculation zone and the (positive) flow within the corner bubble hit each other. A direct comparison with the reference LES data in this region is inadequate because of the reasons explained previously. Present

results exhibit high level of agreement in the recovery region. The evolution of Stanton number ($St = Q_w\Theta_{ref}/(\Theta_w - \Theta_{bulk})$) depicted in Fig. 19 reflects entirely the bulk and wall temperature variations.

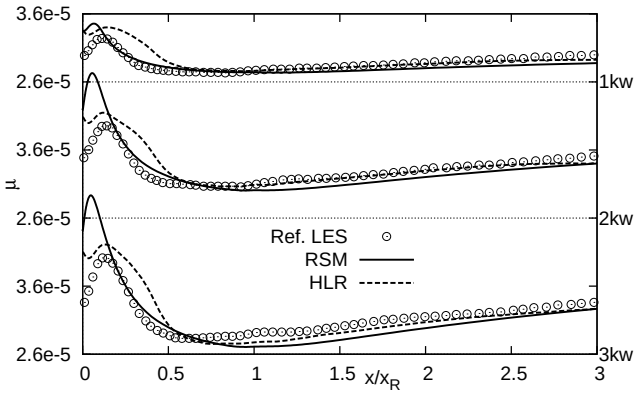

FIGURE 18. Variation of the viscosity for all three cases with wall heating - $q_w = 1$, 2 and $3kW/m^2$

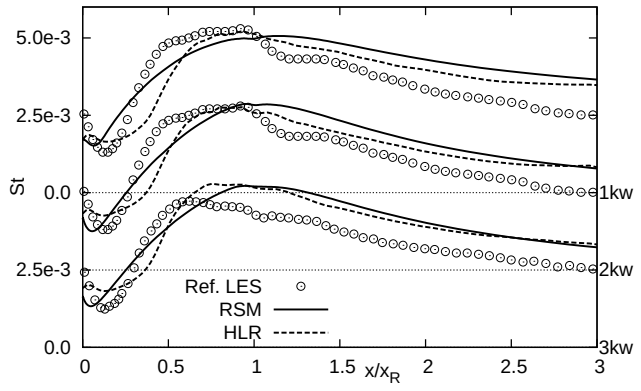

FIGURE 19. Stanton number variation for all three cases with wall heating - $q_w = 1$, 2 and $3kW/m^2$

Laminarizing pipe flow

The strongly-heated, upward air flow in the vertically positioned pipe is considered next. The intensity of the wall heating is illustrated in Fig. 20 displaying the development of the wall temperature and corresponding Nusselt number Nu.

The evolution of the mean velocity profile (Fig. 21, the profiles at three selected locations were shown: $x/D = 3.2$,

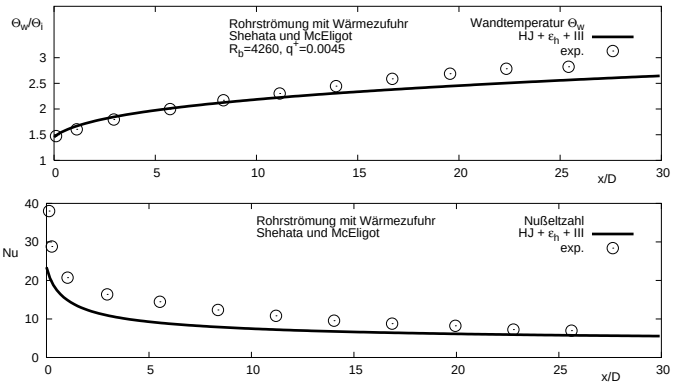

FIGURE 20. Wall temperature development and Nusselt number distribution in a finite-length pipe flow with strong heating

$x/D = 14.2$ and $x/D = 24.5$) indicates clearly the laminarizing features of the upward flow in the vertically positioned pipe. Whereas at the first position investigated a short logarithmic region still exists the profiles at the remaining locations exhibit laminar-like shapes. The mean temperature profiles displayed in Fig. 22 show also reasonable agreement with the experimental results. The substantial growth of the thermal boundary layer thickness obtained with the present model follows closely the experimental results. In Fig. 23 the profiles of the streamwise and the shear stress components including also those corresponding to the isothermal flow situation with respect to the inlet section are presented. Here, the results are compared with the DNS data. One should note that the DNS adopted experimentally obtained wall temperature variation as the boundary condition. The behaviour of both stress components is in accordance with a severe suppression of the turbulence intensity due to local acceleration caused by strong viscosity increase. However, the modelled stress components at two last locations exhibit still significant turbulence level compared to the DNS results.

CONCLUSIONS

The present work displays the potential of a differential, non-linear, near-wall turbulence model on the second-moment closure level associated with different heat flux models of varying complexity in predicting the momentum and heat transfer in a channel flow exhibiting severe fluid property variations due to intensive heating. An important novelty in the turbulence model is the introduction of the homogeneous dissipation rate serving as a new scale supplying variable.

The constant-density flow in a fully-developed channel, serving as a test case for the heat flux models adopted, was predicted in a very good agreement (it is especially related to the model *III* accounting for non-linearities in the pressure-temperature-gradient correlation). Application of the same mod-

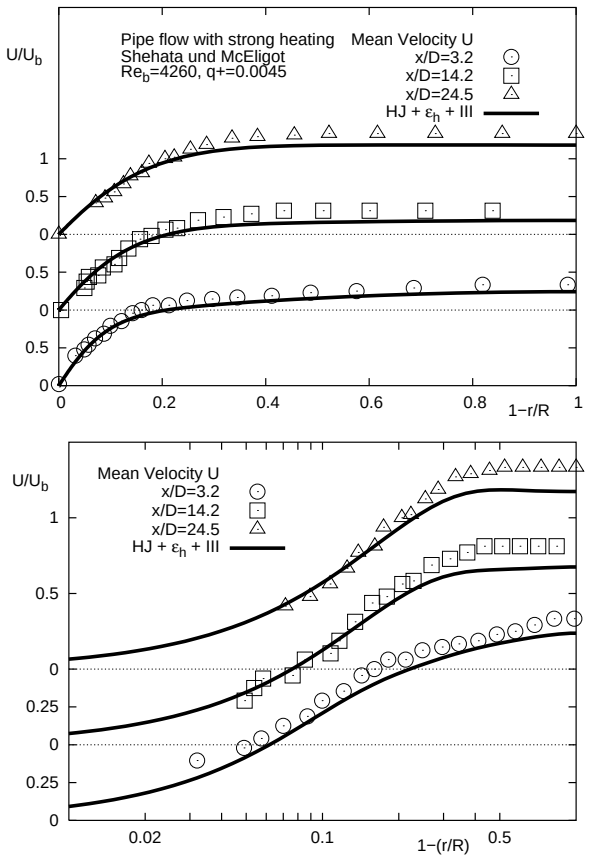

FIGURE 21. Mean velocity profiles at selected positions in a finite-length pipe flow with strong heating

els in a (compressible) flow configuration with variable fluid properties indicated certain deficiencies, being particularly pronounced when predicting the streamwise heat flux component. The reason for this may lie in neglecting the mass flux coupling and pressure dilatation terms. The non-linear pressure-temperature gradient term model (denoted by *III*) is superior to other models applied.

The results obtained by the present RSM model with respect to the reattachment lengths, C_f and Stanton number evolutions, fluid flow and thermal fields follow closely the reference experiment (Kasagi and Matsunaga, 1995) and reference LES (Avancha and Pletcher, 2002) of the backward-facing step flow. This is especially the case in the recovery region. The deviations related to the wall temperature and flow property variations are concentrated mostly in the region of the corner bubble immediately after sudden expansion

Suppression of turbulence due to strong heating in the pipe geometry and associated tendency of the flow to laminarize was returned in a qualitatively good agreement with the reference DNS of Satake (2000). However, the turbulent stress components in the region corresponding to the last third of the pipe length exhibit still a level being significantly higher than predicted by DNS. It seems that the straightforward extension of the incompressible versions of the turbulence models for the Reynolds stresses and heat fluxes to a compressible case characterized by large temperature gradient and the consequent fluid property variations does not suffice here. More modelling activities are required, focusing primarily on the processes which were not accounted for in the Favre-averaged Reynolds stress transport equation such as the pressure dilatation and mass flux coupling.

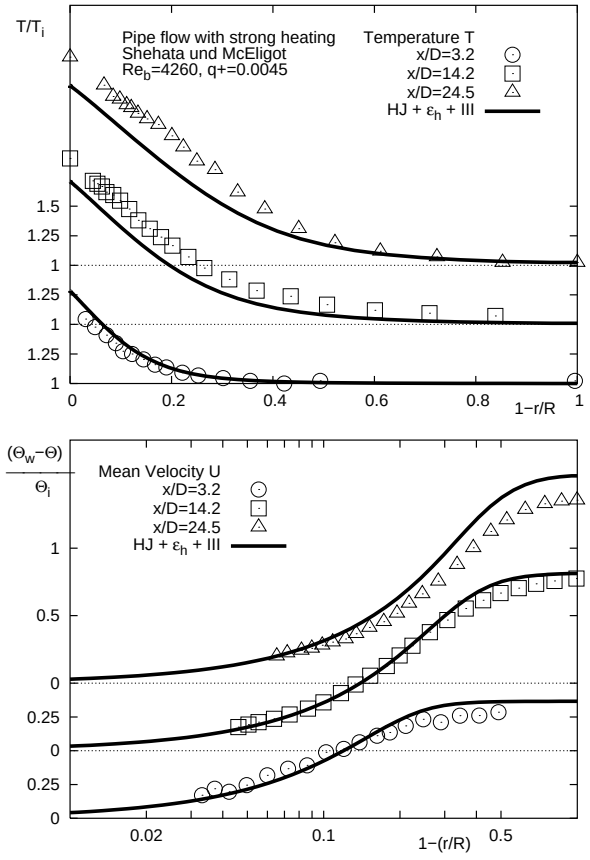

FIGURE 22. Mean temperature profiles at selected positions in a finite-length pipe flow with strong heating

ACKNOWLEDGMENT

The financial support of the Deutsche Forschungsgemeinschaft through the grant SFB568 ”Flow and Combustion in Future Gas Turbine Combustion Chambers” for R. Jester-Zürker is gratefully acknowledged

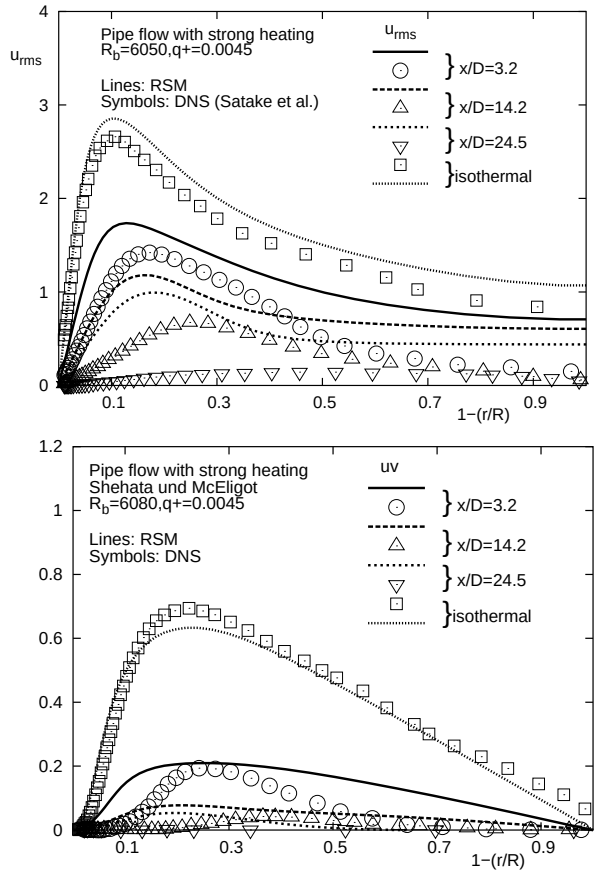

FIGURE 23. Reynolds stress components at selected positions in a finite-length pipe flow with strong heating

References

[1] Avancha, R.V.R., 2001, A study of the heat transfer and fluid mechanics of the turbulent separating and reattaching flow past a backward-facing step using large-eddy simulation, Ph.D. Thesis, Iowa State University

[2] Avancha, R.V.R. and Pletcher, R.H., 2002, Large eddy simulation of the turbulent flow past a backward-facing step with heat transfer and property variations, *Int. J. Heat and Fluid Flow*, Vol. 23, pp. 601-614

[3] Bae, J.H., Yoo, J.Y., Choi, H. and McEligot, D.M., 2006, Effects of large density variation on strongly heated internal air flows, *Phys. Fluids*, Vol. 18, pp. 075102 1-25

[4] Daly, B.J., and Harlow, F.H., 1970, Transport Equations in Turbulence, *Phys. Fluids*, Vol. 13., pp. 2634-2649

[5] Gerolymos, G.A. and Vallet, I., 2002, Wall-normal-free near-wall Reynolds-stress model for 3-D turbomachinery flows. *AIAA Journal*, Vol. 40(2), pp. 199208

[6] Gibson, M.M. and Launder, B.E., 1978, Ground effects on pressure fluctuations in the atmospheric boundary layer. *J. Fluid Mech.*, Vol. 86, pp. 491511

[7] Huang, P. G., Coleman , G. N., and Bradshaw P., 1995, Compressible turbulent channel flows: DNS results and modelling, *J. Fluid Mech.*, Vol. 30, pp. 185-218

[8] Jakirlic, S., and Hanjalic, K., 2002, A new approach to modelling near-wall turbulence energy and stress dissipation, *J. Fluid Mech.*, Vol. 539, pp. 139-166

[9] Jakirlic, S., 2004, DNS-based scrutiny of RANS-approaches and their potential for predicting turbulent flows, Darmstadt University of Technology, Germany

[10] Jones, W. P., 1992, Turbulence modelling for combustion flows. In Modelling for combustion and turbulence, Lecture Series 1992-03, von Karman Institute for Fluid Dynamics

[11] Kasagi, N. and Matsunaga, A., 1995, Three-dimensional particle-tracking velocimetry measurements of turbulence statistics and energy budget in a backward facing step flow, *Int. J. Heat and Fluid Flow*, Vol. 16, pp. 477-485

[12] Kasagi, N., and Iida O., 1999, Progress in direct numerical simulation of turbulent heat transfer, Proc. *5th ASME/JSME Joint Thermal Engineering Conference*, San Diego, CA, USA, March 15-19

[13] Lai, Y. G., and So, R. M. C., 1990, Near-wall modelling of turbulent heat fluxes, *Int. J. Heat Mass Transfer*, Vol. 33(7), pp. 1429-1440

[14] Launder, B.E., Reece, G.J., Rodi, W., 1975, Progress in the development of Reynolds stress turbulence closure. *J. Fluid Mech.*, Vol. 68, pp. 537-566,

[15] Le, H., Moin, P. and Kim, J., 1997, Direct Numerical Simulation of Turbulent Flow over a Backward-Facing Step, *J. Fluid Mech.*, Vol. 330, pp. 349-374

[16] Moser, R.D., Kim, J., Mansour, N.N., 1999, Direct numerical simulation of turbulent channel flow up to $Re_\tau = 590$. *Phys. Fluids* Vol. 11(4), pp. 943-945

[17] Satake, S., Kunugi, T., Shehata, A.M. and McEligot, D.M., 2000, Direct numerical simulation for laminarization of turbulent forced gas flows in circular tubes with strong heating. *Int. J. Heat and Fluid Flow*, Vol. 21, pp. 526-534

[18] Seki, Y., Kawamoto, N., and Kawamura, H., 2003, Proposal of turbulent heat flux model and its application to turbulent channel flow with various thermal boundary conditions, *Turbulence, Heat and Mass Transfer*, Vol. 4, Hanjalic et al. (Eds.), Begell House Inc., pp. 569-576

[19] Shehata, A.M. and McEligot, D.M., 1998, Mean structure in the viscous layer of strongly-heated internal gas flows. Measurements. *Int. J. Heat and Mass Transfer*, Vol. 41, pp. 4297-4313

[20] Speziale, C.G., Sarkar, S., Gatski, T.B., 1991, Modelling the Pressure-Strain Correlation of Turbulence: an Invariant Dynamical Systems Approach. *J. of Fluid Mech.*, Vol. 227, pp 245-272

[21] Wang, W.-P., and Pletcher R., 1996, On the large eddy simulation of a turbulent channel flow with significant heat transfer, *Phys. Fluids*, Vol. 8(12), pp. 3354-3366